



Fast STEM Spectrum Imaging Using Simultaneous EELS and EDS in Gatan Microscopy Suite®

Paolo Longo, Gatan, Inc.

ANALYTICAL TEM APPLICATION NOTE

Up to now, researchers performing analytical investigations in the transmission electron microscope typically had to choose between analytical spectroscopy techniques. They might choose energy dispersive [X-ray] spectroscopy (EDS) analysis when working with thick samples containing high-Z elements, or choose electron energy-loss spectroscopy (EELS) when studying low-Z species in thin samples. With the advent of STEM instruments with both high-mechanical stability and high-brightness probes, coupled with the latest generation of fast, efficient X-ray and EELS detectors, choosing among complementary techniques is a significant restriction. The acquisition systems available up to now have forced a choice because EELS, EDS, and fast scanning have not been designed to work together, resulting in inefficient data collection once the acquisition time per pixel dropped below a few tenths of a second.

In this paper, we present a data collection system that is designed to allow EELS, EDS and dark field detectors to operate efficiently at spectral rates over 1 kHz. This is achieved by allowing each detector system to acquire data independent of the other. The data collection systems are, however, linked together by a synchronization clock pulse to ensure the resulting datasets are in exact spatial alignment. The system described here has been recently implemented using Digital Micrograph together with the Bruker Esprit EDS system. The necessary timing precision is achieved by hardware-synchronizing the EELS and the EDS spectrometers with the beam scanning system as shown schematically in Figure 1. During simultaneous spectral acquisition, the EELS spectrometer provides system synchronization by means of a clock pulse at the end of each acquired frame. This pulse is used to advance the beam position and to inform the EDS system that the pixel has advanced. The EELS and EDS data is stored locally in software buffers and transferred asynchronously to the host application to ensure no data is lost. This mode of acquisition can be performed with any combination of the available signals and is also compatible with other features such as DualEELS acquisition and spatial drift correction.

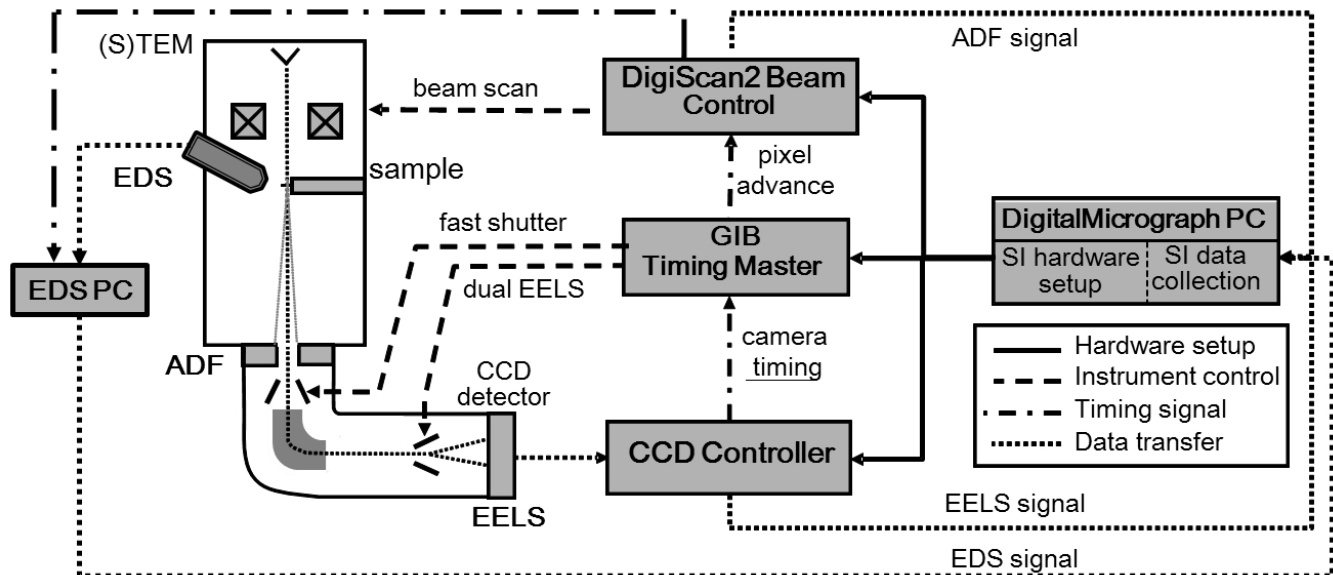
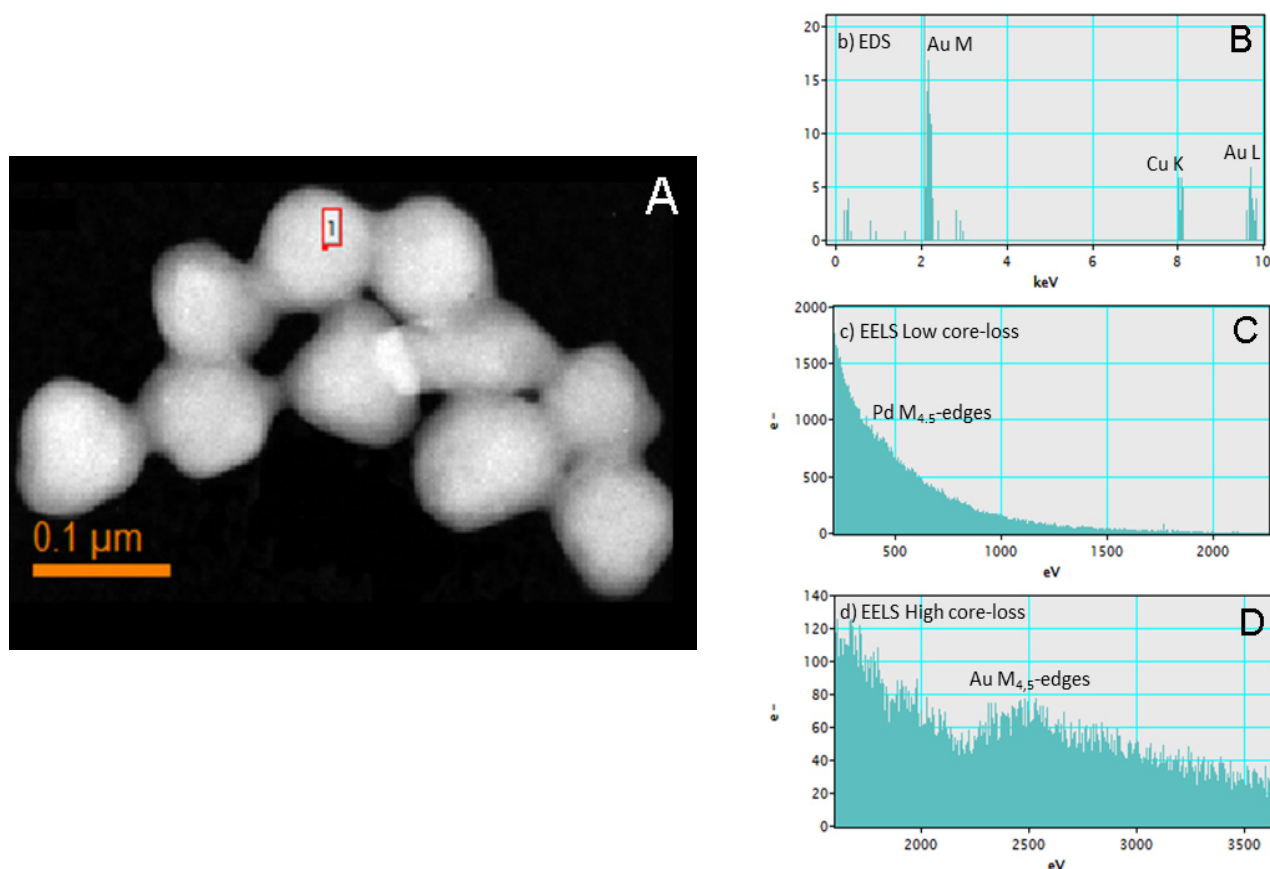


Figure 1: Control signal and data path for joint high-speed EELS and EDS data acquisition. Hardware setup and data transfer are handled asynchronously while the instrument control and timing signals are controlled via a master timing system ensuring all data stays in perfect synchrony and no data is lost.

To illustrate these advances, data was acquired at TU-Graz in Austria using a probe corrected FEI Titan G3 STEM equipped with X-FEG high-brightness electron source operating at 300 kV. The instrument is also equipped with 4 quadrant SDD detector (FEI Super-X) controlled by the Bruker Esprit system and a GIF Quantum ERS imaging filter for EELS acquisition. The EELS spectrometer is configured with the following features: (a) DualEELS™ capability which allows two different regions of the EELS spectrum to be recorded nearly simultaneously ($\Delta t = 10\mu\text{s}$); (b) a low dispersion mode which allows EELS data to be recorded with an energy range up to 2000 eV (or 4000 eV in DualEELS mode); (c) a fast 2-k CCD which allows EELS acquisition at over 1000 spectra per second; and (d) dodecapole lens system capable of correcting spectral aberrations up to the 5th order allowing collection angles well over 100 mrad to be used while maintaining sub-eV energy resolution. The sample analyzed consisted of Pd/Au catalyst nanoparticles kindly provided by Professor Jianfang Wang's group at the Chinese University of Hong Kong. The particles were deposited on a carbon film supported on a Cu mesh TEM grid. Data was acquired using a 220 pA STEM probe as indicated by the microscope fluorescence screen. The STEM is capable of much higher currents, but a relatively low current was needed to minimize sample motion cause by local heating. The probe convergence angle was 20 mrad and the collection angle was 35 mrad. Four different signals (ADF, EDS, EELS high core-loss and low core-loss) were recorded simultaneously. The EELS spectrum image (SI) was acquired in DualEELS™ mode; the regions of the EELS spectrum from 200 eV to 2200 eV and 1800 eV to 3800 eV were acquired using acquisition times of 7 ms and 30 ms respectively. EDS spectra were acquired simultaneously, integrating counts over the entire pixel time employed for the EELS acquisition. This resulted in an EDS pixel time of 39 ms and nearly 100% live time. The count rate was approximately 15k counts/s in the center of a typical Au particle.

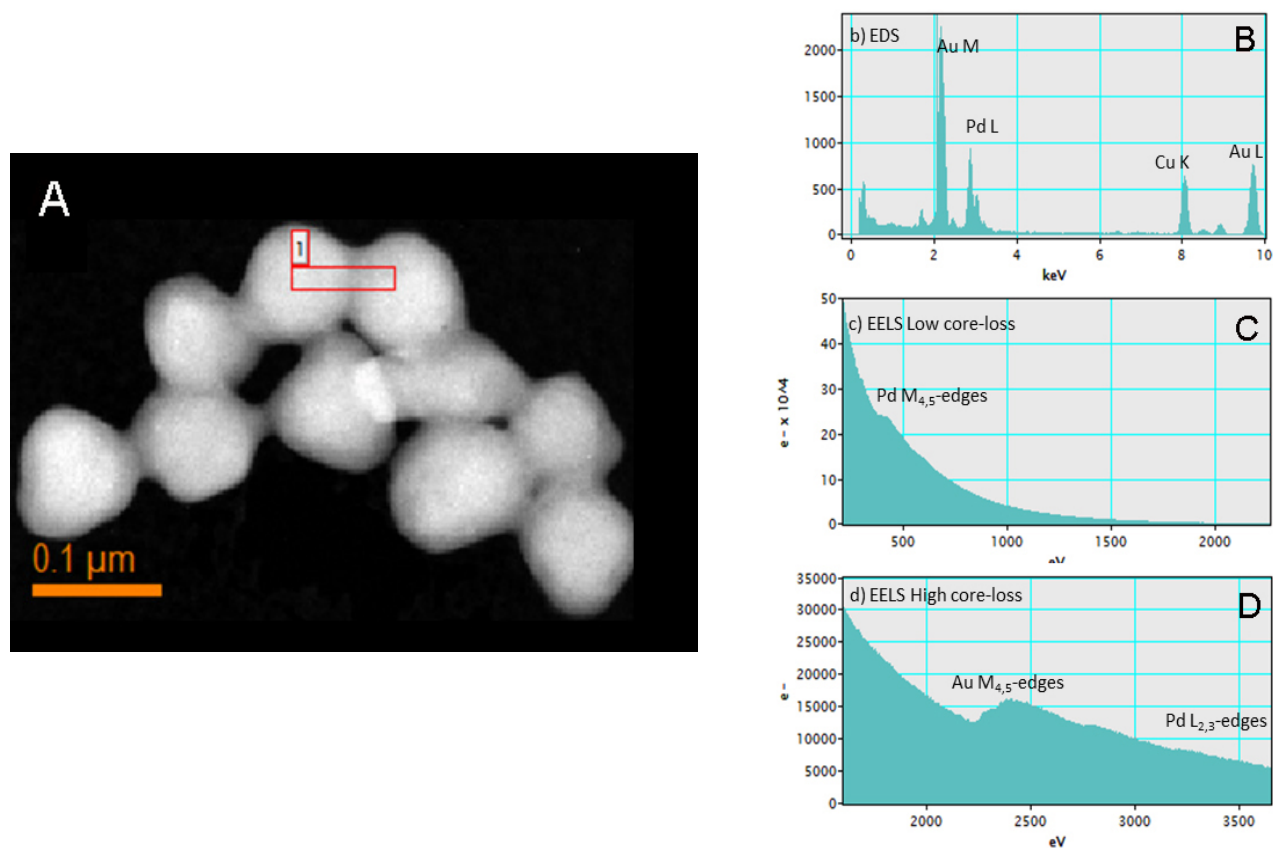
Figures 2B-D show EDS and high and low core-loss EELS spectra from a single pixel extracted from the region shown in Figure 2A. The EELS spectra show a good amount of signal; the Au $M_{4,5}$ -edges at 2206 eV stand out well above the background and a small amount of Pd is evident. The EDS data shows Au X-rays as well as Cu fluorescence.



Figures 2A-D: A: ADF image a simultaneous with the EELS and EDS data showing the location of a single extracted data point. B: EDS data from selected point. C: Low core-loss. D: High core-loss EELS data from the same point. The EELS data indicated only Au and a slight amount of Cu are present. The EDS shows Au as well as Cu from the nearby support.

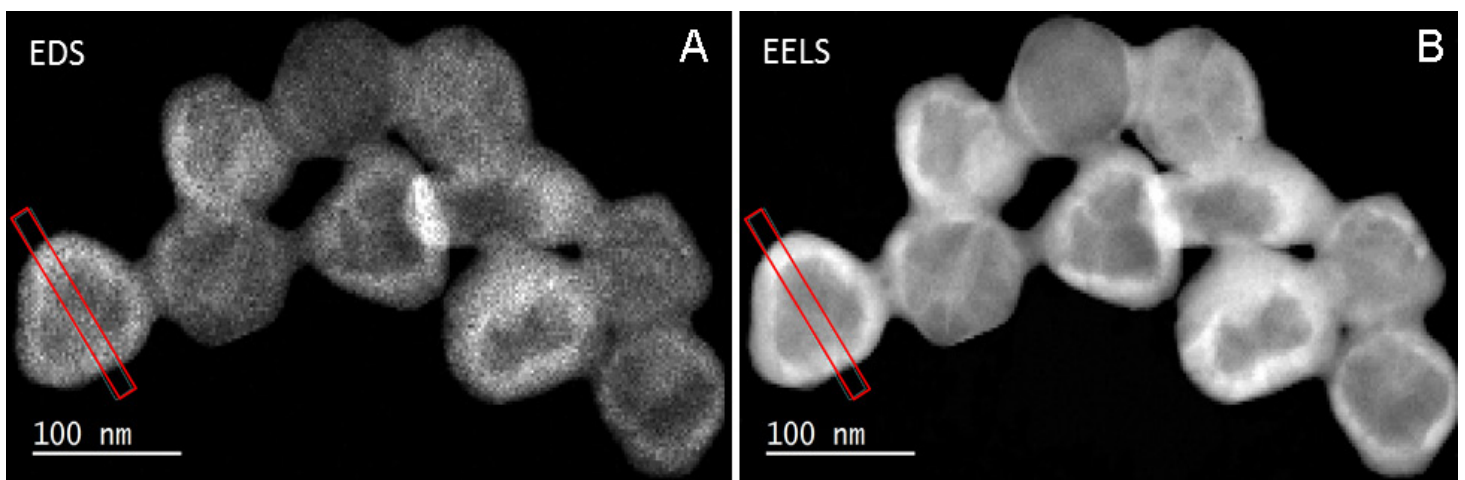
The quality of the spectra for both EELS and EDS dramatically improve after summing adjacent pixels together as shown in Figures 3B-D where 168 pixels across the region shown in Figure 3A were summed. In the summed EDS spectrum, the lines for all the elements present in the sample are observed and also in the Cu supporting grid as a result of poor localization of the EDS signal. The lack of a Cu $L_{2,3}$ edge at 931 eV in the EELS data verifies the nature of the EDS artifact. The EELS low and high core-loss spectra appear to be virtually noiseless due to the very high counting statistics in the data. The Pd $M_{4,5}$ -edges at 335 eV appear to be very strong as well as the Au $M_{4,5}$ -edges at 2206 eV in the high core-loss spectrum. It is also interesting to note there is sufficient signal in the summed EELS data that the high energy Pd $L_{2,3}$ -edges at 3170 eV are also well above the background level and can be used for analysis if needed.

These results demonstrate that when the EELS system and STEM are properly configured, high-energy edges can be recorded with high signal-to-noise ratio using short exposure times. This illustrates the suitability of EELS as a technique to analyze materials containing heavy metals such as Au.



Figures 3A-D: Same data as Figure 2 but for the summation of 168 adjacent pixels containing both Au and Pd.

Figures 4A and 4B show the Pd elemental maps for EDS and EELS, respectively. In the case of EDS, the map was extracted using the La lines at 2.84 kV using an empirical Kramers background fitting followed by multiple linear least square (MLLS) fitting of each peak family represented by a set of Gaussian peaks. In the EELS case, the Pd $M_{4,5}$ -edges at 335 eV was used. The signal overlap with C K-edge of the underlying support film at 284 eV is easily separated using MLLS fitting. MLLS curve fitting of the overlap is only possible when the signal-to-noise ratio for each individual pixel is sufficiently high as is the case in the EELS data. The EELS elemental map for the Pd looks much sharper and shows higher contrast than the same map obtained using EDS. This can be directly attributed to the strong forward scattering of the EELS signal and the nearly 100% collection efficiency of detector. The high signal to noise ratio in the data is evident from intensity line profiles (5 pixel wide average) shown in Figure 5. The profiles are extracted from the region indicated in the red box in the EDS and EELS Pd elemental maps of Figure 4.



Figures 4A-B: Pd Elemental maps: A: EDS. B: EELS. The area in the red box is where the intensity line profiles in Figure 5 were extracted.

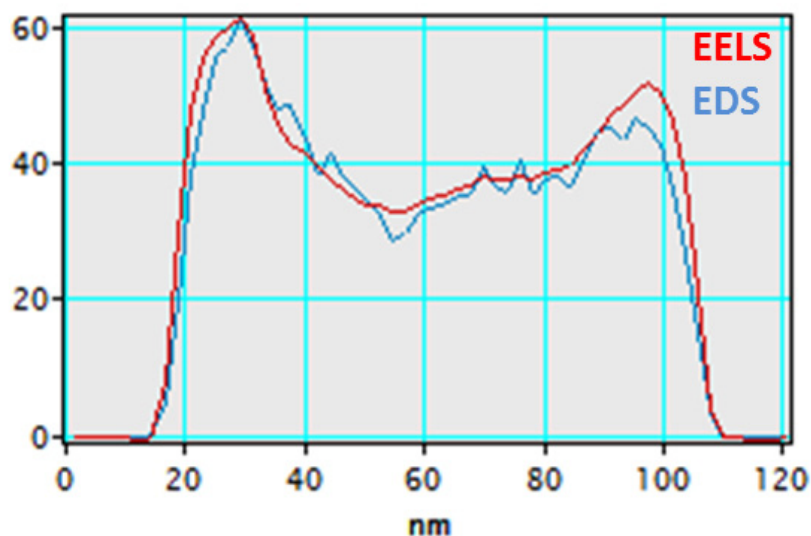


Figure 5: Intensity line profiles extracted from the region in the red box in the Pd elemental maps obtained using EDS and EELS. Lines were superimposed and normalized to the same maximum.

Figures 6A and 6B show the Au elemental maps obtained using EDS and EELS, respectively. In the case of EDS the elemental map was obtained using the Au $M\alpha$ line at 2.12 kV using the fitting procedure as defined above. The EELS Au $M_{4,5}$ -edges at 2206 eV were extracted using power law background fitting. For Au, there is also higher quality in the EELS elemental map compared to that from EDS, despite the copious flux of X-rays from a heavy element such as Au. The Au elemental map obtained using EELS is sharper and shows more details than the same map using EDS.

To measure the relative quality of each map, the signal intensity was analyzed from a uniform region of a Au particle. This 16x16 pixel region is shown by the red box in figure 6 and the extracted data is summarized in Table 1. The SNR for the EELS data is ~17 while that for the EDS data is ~8 giving about a 2x improvement for the EELS data. However, for the EDS data, the SNR is largely limited by counting statistics (noise is approximately equal to the square root of the signal), while the EELS data is limited by the total signal (Au M edge + underlying background). This shows the clear difference between signal-to-noise ratio (SNR) and signal- (or peak-) to-background ratio (P/B). P/B determines what is possible to measure from a sufficiently long exposure while SNR determines what can be extracted from any given data set. For the data measured in this experiment, the EELS signal is more than twice as sensitive than the EDS data. Increasing either the collection efficiency or the dwell time for the EDS signal by a factor of 4 is required to match the EELS signal in this dataset.

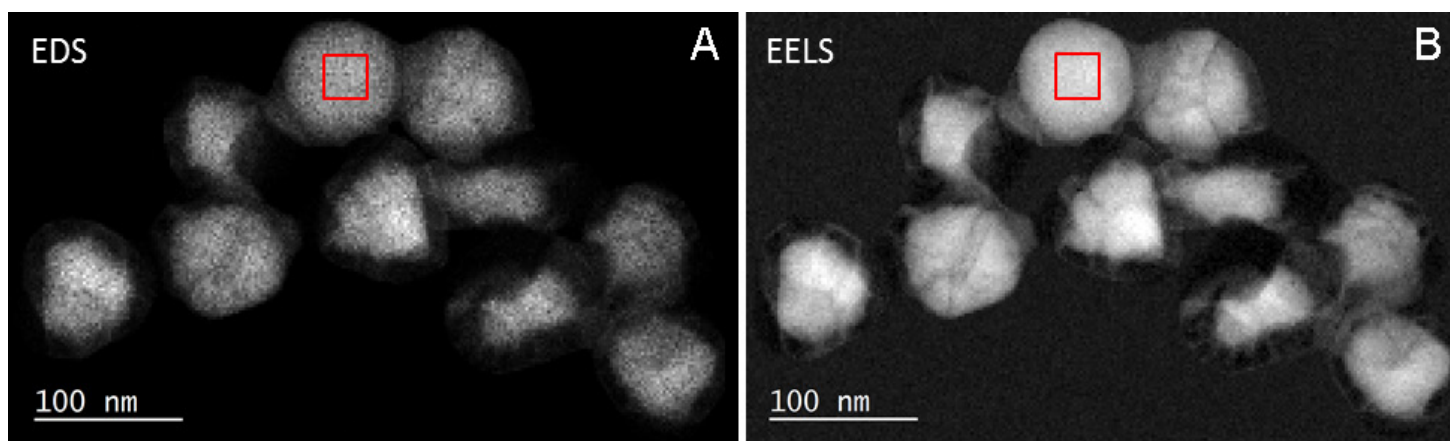


Figure 6A-B: Au Elemental maps: A: EDS. B: EELS. The red box indicates the area used to calculate the map signal to noise ratio.

	Mean signal	Std. Dev.	SNR
Au M EELS Map	14468 counts	856 counts	17:1
Au M EDS Map	79.9 counts	10.1 counts	7.9:1

Table 1: Signal to noise ratio measurements.

Figures 7A and 7B show colored elemental maps of Pd and Au obtained using EDS and EELS respectively. Qualitatively, the EELS maps appear to be sharper and show much higher contrast. In particular, significant details are absent in the EDS maps which are clear in the EELS maps. For example, the diffusion of the Pd into the Au region is difficult to discern in the EDS maps whereas this appears to be clear in the EELS maps.

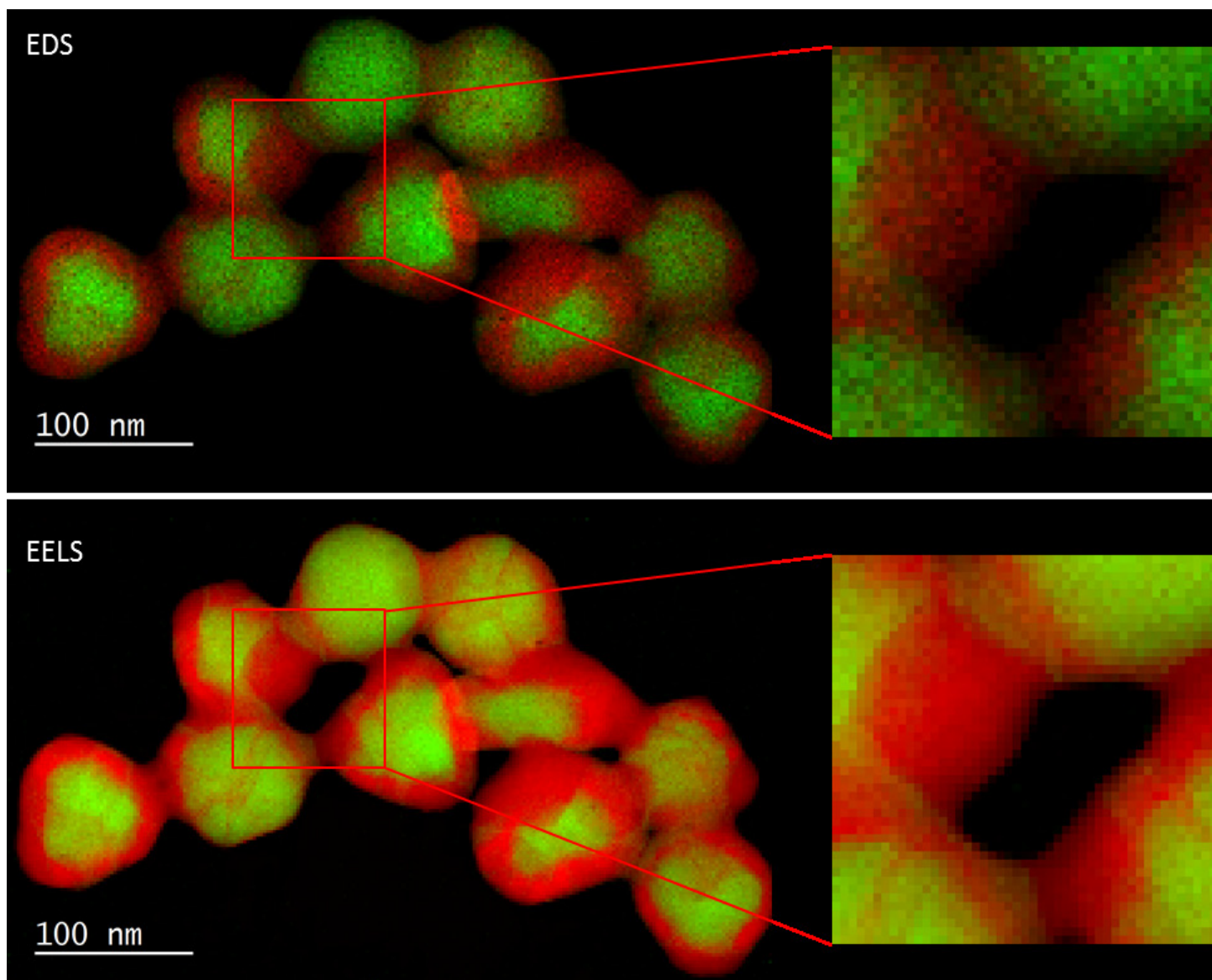


Figure 7: Colorized elemental maps of Pd in red and Au in green acquired using EDS and EELS. The inset is the enlarged image of the region in the red box

The EELS and EDS data presented here can be regarded as highly complementary. The main difference is that for the EDS case, each pixel carries little information due to the very low signal-to-noise ratio of the data even at these long exposure times and with high fluorescence yield materials. However, the high signal-to-background ratio of the EDS technique allows summation of adjacent data almost indefinitely improving the detection limits at the expense of spatial resolution. The EELS data, on the other hand, has very high collection efficiency resulting in high signal-to-noise ratios for each pixel acquired. Summing adjacent pixels improves the detection limits considerably but will show diminishing returns once the shot noise in the signal integral becomes irrelevant. The techniques further complement each other when identifying artifacts in the data. For example, secondary fluorescence and preferential absorption in the EDS data can be determined from the EELS data, while possible missing elements in the EELS data range acquired can be identified in the summed EDS signal.

Having a system for fast and efficient acquisition of both EELS and EDS spectra allows the routine collection of both of these complementary data signals. There is no longer a need to choose between analytical techniques; both EELS and EDS can be acquired easily with every data run. The data presented here shows the complementary nature of having both high signal-to-noise and high signal-to-background data acquired at the same location at the same time. Further, the ability of combining composition measurements from EELS and EDS with physical and electronic information also available only from EELS (e.g. plasmonic, band gap and density of states information) promises to open whole new avenues of materials analysis.



Worldwide Sales Offices

**Gatan, Inc.
Corporate Office**
5794 W. Las Positas Blvd.
Pleasanton, CA 94588 USA
tel +1.925.463.0200
fax +1.925.463.0204
info@gatan.com

Gatan, Inc.
780 Commonwealth Dr.
Warrendale, PA 15086 USA
tel +1.724.776.5260
fax +1.724.776.3360
info@gatan.com

Gatan UK
25 Nuffield Way
Abingdon Oxon
OX14 1RL United Kingdom
tel +44.1235.540160
fax +44.1235.540169
ukinfo@gatan.com

Gatan GmbH
Ingolstädterstr. 12
D-80807 München Germany
tel +49.89.358084-0
fax +49.89.358084-77
gatangmbH@gatan.com

Gatan Singapore
10 Eunos Rd. 8 #12-06
Singapore Post Centre
Singapore 408600
tel +1.65.6408.6230
fax +1.65.6293.3307
gatansingapore@gatan.com

Nippon Gatan
3F Sakurai bldg. 2-8-19
Fukagawa, Koto-ku Tokyo
135-0033 Japan
tel +81.3.5639.2772
fax +81.3.5639.2763
nippongatan@gatan.com

Gatan France
ROPER Scientific-Division
Gatan
8, rue du Forez-CE 1702
ZI petite Montagne Sud
91017 EVRY Cedex
France
tel +33.1.69.11.03.69
fax +33.1.64.97.19.67
gatanfrance@gatan.com

